Toxicology and Applied Pharmacology 486 (2024) 116937

Contents lists available at ScienceDirect

Toxicology and Applied Pharmacology

journal homepage: www.elsevier.com/locate/taap

Dysregulation of adipogenesis and disrupted lipid metabolism by the antidepressants citalopram and sertraline

Deniz Bozdag [a,b], Jeroen van Voorthuizen [a], Nikita Korpel [a], Sander Lentz [a], Hande Gurer-Orhan [b], Jorke H. Kamstra [a,*]

[a] Faculty of Veterinary Medicine, Department of Population Health Sciences, Institute for Risk Assessment Sciences, Utrecht University, 3584 CM Utrecht, the Netherlands
[b] Faculty of Pharmacy, Department of Pharmaceutical Toxicology, Ege University, 35040 Izmir, Turkey

ARTICLE INFO

Editor Name: Lawrence Lash

Keywords:
Citalopram
Sertraline
In vitro
Adipogenesis
Lysosome
Phospholipid

ABSTRACT

Selective Serotonin Reuptake Inhibitors (SSRIs) are widely used medications for the treatment of major depressive disorder. However, long-term SSRI use has been associated with weight gain and altered lipid profiles. These findings suggest that SSRIs may have negative effects on metabolism. Exposure to certain chemicals called 'obesogens' is known to promote lipid accumulation and obesity by modulating adipogenesis. Here, we investigated whether citalopram (CIT) and sertraline (SER) interfere with the process of adipogenesis, using human mesenchymal stem cells (MSCs) in a 2D and a 3D model. Assessment of intracellular lipid accumulation by fluorescence staining was used as a measure for enhanced adipogenesis. To explore possible mechanisms behind SSRIs' effects, receptor mediated activity was studied using responsive cell lines for various nuclear receptors. Furthermore, RNA sequencing was performed in the 3D model, followed by differential gene expression and pathway analysis. A dose dependent increase in lipid accumulation was observed in both models with CIT and SER. For the 3D model, the effect was seen in a range close to reported steady-state plasma concentrations (0.065–0.65 μM for SER and 0.12–0.92 μM for CIT). Pathway analysis revealed unexpected results of down-regulation in adipogenesis-related pathways and upregulation in phospholipids and lysosomal pathways. This was confirmed by an observed increase in lysosomes in the 2D model. Our findings suggest lysosomal dysfunction and disrupted lipid metabolism in mature adipocytes, leading to excessive phospholipid synthesis. Moreover, important adipogenic processes are inhibited, potentially leading to dysfunctional adipocytes, which might have implications in the maintenance of a healthy metabolic balance.

1. Introduction

Selective serotonin reuptake inhibitors (SSRIs), used in the treatment of moderate to severe major depressive disorder (MDD), are among the most used medications worldwide. Recent evidence suggests a link between long-term SSRI treatment and weight gain in adults, including two of the most prescribed SSRIs, citalopram (CIT) and sertraline (SER) (Arterburn et al., 2016; Blumenthal et al., 2014; Gafoor et al., 2018; Uguz et al., 2015). Studies report an increase in weight with CIT, ranging from 1.69 kg (≥ 4 months follow-up) to 2.68 kg (24 months follow-up) (Blumenthal et al., 2014; Serretti and Mandelli, 2010), while SER was associated with a weight increase ranging from 1.0 kg (9 months follow-up) to 4.76 kg (24 months follow-up)(Blumenthal et al., 2014; Serretti and Mandelli, 2010). Additionally, there are reports on altered lipid profiles such as increased serum triglyceride levels with CIT (an average increase of 18.89 mg/dL, $p = 0.001$) and total cholesterol levels with SER (an average increase of 3.85 mg/dL, $p = 0.027$) in female patients after 4 months follow-up (Beyazyüz et al., 2013), yet the mechanism behind these effects remains elusive. Although SSRIs are largely considered safe and prescribed to women during pregnancy, there is increasing concern related to their maternal and neonatal safety (Gill et al., 2020; Molenaar et al., 2020; Pariente et al., 2016). Given that CIT and SER are among the most commonly prescribed SSRIs to pregnant women, research on their obesogenic potential and the underlying mechanisms is timely, as these medications might be contributing to the worldwide increase in obesity.

Obesity is characterized by an abnormal and unhealthy accumulation of body fat and has evolved into a pandemic that is affecting people all around the world. In 2022, obesity is observed in 1 in 8 people globally (890 million people of 18 years of age or older) and in >160

* Corresponding author.
E-mail addresses: bozdagde@gmail.com (D. Bozdag), j.h.kamstra@uu.nl (J.H. Kamstra).

https://doi.org/10.1016/j.taap.2024.116937
Received 5 January 2024; Received in revised form 7 April 2024; Accepted 17 April 2024
Available online 20 April 2024

million children and adolescents (between 5 and 19 years of age) worldwide (WHO, 2024). Besides being a serious health concern itself, obesity also acts as a contributing factor in the development of metabolic syndrome, non-alcoholic fatty liver disease (NAFLD), and type 2 diabetes (T2D) (Lustig et al., 2022). The traditional explanation for obesity is an imbalance between caloric intake and expenditure, favoring increased caloric intake (WHO, 2024). However, while energy imbalance and genetics play pivotal roles, they alone cannot explain the increase in obesity rates over the last 40 years (Lustig et al., 2022; Schwartz et al., 2017). This has shifted the focus onto environmental factors, such as chemical exposure, as the cause of the current obesity pandemic. Starting from the early 2000s, there has been growing research on chemicals' influence on adipogenesis, the process of adipocyte differentiation regulated by various transcription factors (Chamorro-García et al., 2013; Chen et al., 2016). Shortly, upon activation by a ligand the main regulator, peroxisome proliferator-activated receptor gamma (PPARγ), initiates adipocyte gene expression, inducing adipocyte differentiation (Janesick and Blumberg, 2016; Kamstra et al., 2014; Sarjeant and Stephens, 2012). As a result of numerous studies, we know today that most of these chemicals, later termed "obesogens" (Grün et al., 2006), activate *PPARγ* in a relatively well-defined mechanism to promote obesity (Blumberg and Egusquiza, 2020; Darbre, 2017; Kamstra et al., 2014; Lustig et al., 2022). Although the PPAR pathway is quite well-known, the knowledge on some of the other mechanisms is still very limited and can widely vary between chemicals (Blumberg and Egusquiza, 2020; Heindel et al., 2022).

The most established model for screening obesogens is the *in vitro* adipogenesis assay using cell lines such as murine preadipocyte cells (3T3-L1) and multipotent mesenchymal stem cells (MSC) (Kassotis et al., 2022; Legler et al., 2020). Although the cell line 3T3-L1 is robust and well characterized, its ability to detect obesogens acting through a different mechanism than PPARγ activation seems to differ between sources and lots (Kassotis et al., 2022, 2021). Human MSCs, offer improved assessment of adipocyte differentiation, by including adipocyte lineage commitment (Kassotis et al., 2022; Legler et al., 2020). Most of the studies use 2D monolayer cultures, yet when comparing 2D grown adipocytes to *in vivo* adipose tissue, significant differences in morphology, size, and transcriptional profiles are observed (Klingelhutz et al., 2018). Recent studies in 3D set-ups have shown 3D adipogenesis models to be more representative of *in vivo* conditions with improved adipocyte differentiation and gene expression (Klingelhutz et al., 2018; Muller et al., 2019; Shen et al., 2021).

Another important aspect that is getting more attention is the question of whether exposure to obesogens leads to functional and "healthy" adipocytes or dysfunctional adipocytes, which in turn has a profound impact on metabolic health (Lustig et al., 2022; Qian et al., 2021). Generally, prototypical *PPARγ* activators, like thiazolidinediones, lead to enhanced adipogenesis, allowing proper functioning of adipose tissue with normal secretion of the insulin-sensitizing, anti-inflammatory, and anti-fibrotic hormone Adiponectin and other adipokines (Ghaben and Scherer, 2019; Heindel et al., 2022). On the other hand, obesogens acting through other mechanisms have been associated with increased insulin resistance and inflammation in the adipose tissue (Ghaben and Scherer, 2019; Qian et al., 2021). An example is the well-studied obesogen tributyltin (TBT), that acts through both PPARγ and its heterodimeric partner, retinoid X receptor (RXR) (Chamorro-García et al., 2013; Li et al., 2011). TBT was shown to decrease glucose uptake and Adiponectin expression in RXR-induced adipocytes, creating a dysfunctional adipocyte with higher risk of progressing into obesity and T2D (Shoucri et al., 2017). Gene expression profiles differed considerably between PPARγ and RXR induced adipocytes, demonstrating transcriptional profiling next to functional readouts could provide valuable insights into obesogens' effects on adipose tissue development and function.

In this context, considering the reported effects on body weight and lipid profiles, suggestive of enhanced fat accumulation and disrupted lipid metabolism, we hypothesized that CIT and SER might induce adiposity, potentially leading to the formation of dysfunctional adipocytes. To test this hypothesis, we used a human MSC model to assess the effects of SSRIs on adipogenesis. To mechanistically explain these effects, we investigated the endocrine modalities using responsive cell lines for various nuclear receptors. We developed and optimized a 3D model, performing transcriptomics analysis to compare the transcriptional profiles of 2D and 3D conditions to characterize the 3D model, as well as further clarifying the underlying mechanism behind SSRIs' effects, *via* functional analyses on nuclear receptors and lysosomes.

2. Materials and methods

2.1. Chemicals

Citalopram hydrobromide and sertraline hydrochloride were purchased from Sigma-Aldrich (Germany). Product details for the SSRIs, the rest of the chemicals and reagents are provided in Supplementary Information S1 (Table S1). Stock solutions for test chemicals were prepared in dimethyl sulfoxide (DMSO, Sigma-Aldrich, Germany) prior to experiments and stored at −20 °C.

2.2. Cell culture

2.2.1. Reporter cell lines

Endocrine-related activity of the SSRIs was tested using reporter cell lines for various nuclear receptors. Potential agonistic/antagonistic activity was tested on estrogen receptor (ER) mediated luciferase reporter gene (ER-Luc) human ovarian carcinoma (VM7Luc4E2) cells (Rogers and Denison, 2000), androgen receptor (AR) mediated luciferase reporter gene (AR-Luc) human breast carcinoma (T47D-ARE) cells (Blankvoort et al., 2001), dioxin/aryl hydrocarbon receptor (DR/AhR) enhanced green fluorescent protein reporter gene (DR-GFP) mouse hepatoma (H1G1.1c3) cells (Nagy et al., 2002), and peroxisome proliferator activated receptor gamma and alpha receptors (PPARγ and PPARα) mediated luciferase reporter gene (PPARγ-Luc and PPARα-Luc) human HeLa cells (HG5LN-hPPARγ and HG5LN-hPPARα) (Seimandi et al., 2005). Cell culture and experimental procedures for the different reporter cell lines are provided in Supplementary Information S2, with differences in methodologies indicated in Table S2.

2.2.2. Adipocyte differentiation from human mesenchymal stem cells

Human bone marrow derived mesenchymal stem cells (hBM-MSCs) from a 61-year-old Caucasian male donor were purchased from PromoCell (Germany) at passage 2 and expanded in the recommended media (MSC Growth Medium 2 with 10% Supplement Mix, PromoCell) according to manufacturer's instructions. Cells were subcultured once after thawing, at 70–80% confluence and frozen in MSC Growth Medium 2 containing 5% DMSO. All experiments were performed at passage 6 (Fig. 1).

MSCs were differentiated into mature adipocytes in 3D and 2D, using similar protocols but with adjustments for the different models. 0.1% DMSO was used as vehicle control, and prototypical PPARγ agonist Rosiglitazone (ROSI) at 0.5 μM was used as a positive control for adipogenesis assays, and for inducing MSC differentiation for the mature adipocyte experiments. Differences in methodologies for the differentiation and analyses are summarized in Table 1.

For 3D experiments, MSCs were seeded in 0.2 mL culture medium (Minimum Essential Medium alpha (MEMα) supplemented with 15% FBS, 1% Penicillin-Streptomycin (P/S), 2% HEPES) in the inner wells of 96 well ultra-low attachment (ULA) plates (Corning® 7007) at 5×10^3 cells per well (adipogenesis, RNA-seq and QPCR assays). The outer rows were filled with PBS. After seeding, ULA plates were centrifuged at 150*g* for 2 min to facilitate the formation of spheroids. During 3D experiments, spheroid formation was confirmed under the microscope two days after seeding and differentiation was induced by replacing half of

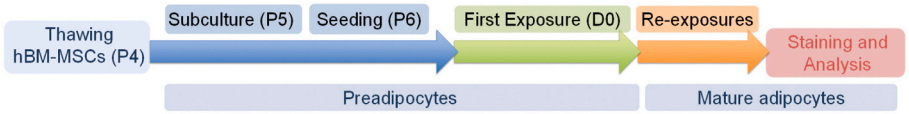

Fig. 1. Experimental design: Schematic representation of the experimental set-up for mesenchymal stem cell (MSC) culture and differentiation in 3D and 2D. First exposure, day 0 (D0), indicates the beginning and re-exposures indicate the refreshment of differentiation medium with the assigned exposures every 3–4 days.

Table 1
Differences in methodologies and analyses for the different adipogenesis assays.

Assay	3D	2D	2D mature adipocytes
Cell culture plates	96 well ultra-low attachment (ULA) Corning®	24 well Greiner Bio-One	24 well Greiner Bio-One
Cell density per well	5×10^3	25×10^3	25×10^3
Seeding volume (mL)	0.2	1	1
Time between seeding and exposures	2 days	4 days	4 days
Differentiation medium conc. (for the first exposure)	2×	1×	1×
Total amount of exposures	5	4	6
Exposure procedure	Replacement of 50% medium, every 3 to 4 days	Replacement of the entire medium, every 3 to 4 days	Replacement of the entire medium, every 3 to 4 days
Assay duration	14 days	14 days	21 days
Analysis method	High-throughput imaging RNA-seq QPCR	Fluorescence plate reader Flow cytometry RNA-seq QPCR	Fluorescence plate reader

the medium (0.1 mL) with 2× differentiation medium (culture medium supplemented with 1 mM 3-isobutyl-1-methylxanthine (IBMX), 0.2 μM dexamethasone (Dex), and 10 μg/mL insulin). Half of the medium was refreshed subsequently with 1× differentiation medium (culture medium supp. With 0.5 mM IBMX, 0.1 μM Dex, and 5 μg/mL insulin) every 3 to 4 days after initial exposure.

For 2D experiments, MSCs were seeded in 1 mL culture medium in 24 well plates (Greiner Bio-One) at 25×10^3 cells per well (adipogenesis, RNA-seq and QPCR assays). Adipocyte differentiation was induced at 100% confluency, four days after seeding, by replacing the entire culture medium with 1× differentiation medium (see above). Differentiation medium with the assigned exposures was refreshed subsequently every 3 to 4 days for 14 days. Cells were exposed to 6 up to 8 concentrations of SER and CIT in a range around reported steady-state plasma concentrations (SSCs); 20–200 ng/mL (0.065–0.65 μM) for SER (De Vane et al., 2002; Ronfeld et al., 1997), and 40–300 ng/mL (0.12–0.92 μM) for CIT (Baumann, 1996; Gutierrez and Abramowitz, 2000; Pollock, 2001).

For the mature adipocyte experiments, cells were first differentiated with 0.5 μM ROSI for 12 days. On day 12, differentiation medium was replaced with culture medium containing only 5 μg/mL insulin, followed by medium refreshments on days 14 and 17 (insulin medium with the assigned exposures, 10 μM SER and 30 μM CIT). Subsequently, cells were fixated and stained for analysis on day 21.

For all experiments, three independent biological experiments were performed for each model (2D and 3D), with the exception of flow cytometry analysis (2D) which was done in two experiments. Each experiment consisted of a maximum of 6 (3D) or 3 (2D) plate replicates.

For transcriptional profiling, cells were exposed to vehicle (DMSO) and positive control (ROSI at 0.1 μM) in 2D and 3D, while chemicals (SER at 0.1–1 μM and CIT at 1–10 μM) were tested in 3D. Three independent experiments were performed for both 2D and 3D models (except for 3D control which is $n = 4$).

2.3. Assessment of adipocyte differentiation

MSCs were analyzed after 14 days of differentiation. For 3D, 50% medium was removed from the wells at every step, therefore 2× concentrated solutions were prepared for the fixation and staining. Cells were fixated with 3.7% formaldehyde (37%, Sigma-Aldrich, Germany) solution in PBS for 30-min, rinsed 2 times with 0.1 mL PBS (again by removal of 50% fluid for the washing steps) and subsequently stained for intracellular lipids with 1 μg/mL Nile Red (Sigma-Aldrich, Germany) and 5 μg/mL Hoechst 33342 (Invitrogen, Thermo Fischer Scientific, NL) for 1.5 h, the given concentrations are the final concentrations in the well. After staining, cells were rinsed 2 times with PBS and left with 0.2 mL PBS per well. Images were taken with a high-content microscope (CellInsight™ CX5 High-Content Screening (HCS) Platform (Thermo Scientific) of each spheroid at 10× magnification. Nile Red was imaged in the FITC channel (Ex 482/35, Em 536/40) and Hoechst in the DAPI channel (Ex 377/50, Em 447/60) and analyzed using CellProfiler software (v4.2.4) (Stirling et al., 2021). Analysis pipeline is provided as supplementary.

For 2D, Nile Red fluorescence was measured either with a fluorescence plate reader (Tecan, Infinite M2000) or flow cytometry (Accuri C6 Flow Cytometer, BD Biosciences, NL). A similar fixation/staining procedure to 3D was performed for fluorescence plate reader, but by refreshment of the entire medium at every step, therefore preparing 1× concentrated solutions in PBS. Cells were first fixed with 3.7% formaldehyde solution in PBS for 30-min, rinsed 2 times with 0.5 mL PBS and subsequently stained with 10 μg/mL Nile Red and 0.5 μg/mL Hoechst for 1.5 h. Nile Red fluorescence was measured at Ex/Em 485/590 nm and Ex/Em 585/645 nm for neutral and phospholipids, respectively, with Hoechst at Ex/Em 355/460 nm for cell number.

For flow cytometry analysis exposure medium was aspirated and cells were rinsed with 0.5 mL PBS, trypsinized (0.25 mL) for 10-min. After cell detachment was confirmed under the microscope, 0.75 mL freshly prepared buffer (Milli-Q water containing 1% Bovine Serum Albumin (BSA), 2 mM EDTA (ethylenediaminetetraacetic acid) and 0.025 μg/mL Nile Red) was added to each well, cells were resuspended by pipetting up and down and incubated for at least 10-min. Half of the plate was measured at a time, cells were resuspended again to prevent clogging of the machine. Neutral and phospholipid accumulation was assessed using the Accuri C6 flow cytometer (BD Biosciences, NL). Flow cytometry analysis was performed by using the positive control ROSI as a basis for the gating strategy. The first gating (P1) was for separating cells from debris, based on SSC-A (side scatter-area)/FSC-A (forward scatter-area). Cells were further sorted according to lipid profiles (P2) based on Nile Red intensity, optical filters FL2 (Em 585/40) and FL3 (Em > 670) were used for neutral and phospholipids, respectively.

2.4. Lysosome analysis

In the 2D model, we performed additional experiments for functional read-outs in the model, starting with measuring SSRIs' effects on lysosomes during differentiation. We used a cell permeable dye that stains acidic compartments, LysoTracker Red DND-99 (Invitrogen, Thermo

Fischer Scientific, NL), and used Amiodarone (AMIO), a broad-spectrum antiarrhythmic drug and a known inducer of phospholipidosis (Reasor et al., 2006), as positive control.

For the experiments, MSCs were differentiated in 2D as previously described. After 14 days of differentiation, cells were live stained with 100 nM LysoTracker Red for lysosomes and 0.5 μg/mL Hoechst for cell nuclei. Staining solution was prepared in culture medium, according to manufacturer's instructions, cells were incubated with LysoTracker Red for 1.5 h at 37 °C and 5% CO_2. After staining, cells were rinsed 2 times with 0.5 mL PBS and left with 1 mL PBS per well. LysoTracker fluorescence was measured using a fluorescence plate reader (Tecan, Infinite M2000) at Ex/Em 565/599 nm, and Hoechst at Ex/Em 355/460 nm. Three independent experiments were performed with three plate replicates for each experiment (2D).

2.5. Brightfield and confocal imaging

MSCs were fixed as described above. 3D spheroids were cut into 10 μm sections using a cryostat and stained with Hematoxylin and Eosin (H&E) for imaging. For cryosectioning, spheroids that were exposed to control and ROSI ($n = 6$) were transferred from the 96 well plate to microcentrifuge tubes. Excess PBS was removed and 0.2 μL KP cryocompound was added to the tube. A cryomold was prepared by freezing two layers of clear colored KP cryocompound at −20 °C and the KP cryocompound containing spheroids was transferred to the cryomold. A new layer of yellow colored KP cryocompound was added on top to embed the spheroid. A cryostat (Leica CM3050s) was used to cut 10 μm sections of the spheroids. The sections were transferred to SuperFrost Plus, Adhesion Slides (VWR, NL) and dried overnight. For H&E staining, slides were incubated in distilled water for 30s; hematoxylin solution for 2-min; eosin solution for 10s and rinsed with 95% ethanol for 30s. Followed by two-times 30s incubation in absolute ethanol and 2-min incubation in xylene. All slides were cover slipped with Entellan mounting medium and dried overnight. Pictures were taken with the Olympus BX60 WF microscope under 20× magnification.

For fluorescence imaging, stained MSCs (see above) were used. Nile Red was imaged in the FITC channel (Ex 482/35, Em 536/40) and Hoechst in the DAPI channel (Ex 377/50, Em 447/60). 3D spheroids were imaged with Olympus/Evident Spin IXplore SoRa microscope under 20× magnification. 2D adipocytes were imaged with Leica DM IL LED microscope using LAS X software, under 20× magnification.

2.6. RNA-seq analysis

For RNA-seq analysis, MSCs were seeded in 24 (2D) or 96 (3D) well ultra-low affinity plates, as described above. In order to characterize the 3D model, cells were exposed to control (0.1% DMSO) or positive control (0.1 μM ROSI) in 2D and 3D. CIT and SER were tested at their NOEC (no observed effect concentration) and LOEC (lowest observed effect concentration) in the 3D model (CIT at 1–10 μM, SER at 0.1–1 μM). 3 independent biological experiments were performed for both 2D and 3D, with one extra control for 3D.

After exposures, total RNA was isolated and purified using the NucleoSpin® RNA extraction kit (Macherey-Nagel, Germany) from one confluent well of a 24 well plate or a pool of 10–20 spheroids. RNA integrity number (RIN) was determined with Agilent 2100 Bioanalyzer (Agilent Technologies, Ca, USA) using RNA Nano LabChip Kit (Agilent Technologies, Ca, USA). All samples were found to be of acceptable quality for sequencing (RIN > 9.0) and sent to Novogene (UK) for sequencing by poly-A capture, library preparation and analysis on the Illumina Novaseq using 150 bp paired end sequencing. Raw fastq files were adapter trimmed using trim_galore (v0.4.5, Babraham institute, UK) under standard parameters. STAR aligner (v2.5.4 b) was used to align and map sequences to the *homo sapiens* genome (GRCh38_v102 https://www.ensembl.org) (Dobin et al., 2013). Mapping data is provided in Table S3. After alignment, the generated BAM files were loaded to SeqMonk sequence analysis tool (v1.41, Babraham Institute, UK) and mRNAs were quantified using the built-in mRNA seq pipeline. Data quality plots were generated, and all data was found to be of acceptable quality (Fig. S1 and S2). Clustering of the individual samples based on model and treatment is shown in Fig. S3. Normalization of the read counts and differential expression was conducted using the Deseq2 method (Love et al., 2014). The data discussed in this publication has been deposited in NCBI's Gene Expression Omnibus (Edgar et al., 2002) and is accessible through GEO Series accession number GSE242103 (https://www.ncbi.nlm.nih.gov/geo/query/acc.cgi?acc= GSE242103).

Differentially expressed genes (DEGs) were scored based on their *p*-value and shrunken log2 fold changes and imported to Webgestalt (Liao et al., 2019) for gene set enrichment analysis (GSEA) using KEGG (Kyoto Encyclopedia of Genes and Genomes) pathway and gene ontology (GO) databases. GSEA parameters were adjusted to only include pathways containing a minimum of 5 and a maximum of 200 genes per pathway. Subsequently, pathways were selected based on FDR values where at least one of the individual treatments exhibited a significant change (FDR < 0.05). For 2D *vs* 3D model comparisons, pathways that were significantly altered with ROSI treatment were used. We used normalized enrichment scores (NES) for a more accurate comparison of the enriched pathways with different gene numbers (Xie et al., 2021). Functional networks were constructed in Cytoscape (v 3.9.1) using the ClueGO (v 2.5.9) and CluePedia (v 1.5.9) plugins (Bindea et al., 2009). Significant KEGG and GO pathways of each condition were imported to perform a Preselected Functions analysis using the KEGG and GO biological processes ontologies (v 16-05-2023). GO term fusion was enabled to prevent duplicate pathways.

For further exploration of the RNA-seq data, DEGs were selected for either one of the treatments in 3D ($n = 3848$) and clustered using the k-means method (Cluster 3.0) (Koch et al., 2018). Silhouette score was used to determine the optimal number of clusters and evaluate the quality of clustering. DEG lists of clusters were imported to Webgestalt for over representation analysis (ORA) with KEGG pathways, using the complete gene list as reference set (parameters were kept the same as the GSEA, see previous section). Representative pathways were selected from each cluster and violin plots were generated with median-adjusted normalized counts of the underlying genes. Top 20 DEGs from each representative pathway were selected (based on significance and meaningful expression levels) and visualized as a heatmap. Violin plots and heatmap are generated using GraphPad Prism (v9.0).

2.7. QPCR analysis

We performed QPCR analysis for selected adipogenic genes to confirm the results of the RNA-seq. MSCs were seeded in 96 well ultra-low affinity plates as described above and differentiated in 3D. Cells were exposed to the same conditions as the RNA-seq (see above) in 2 independent biological experiments.

After the exposures, RNA isolation and purification was performed (as described for RNA-seq analysis). RNA amount of the samples was not measured, due to low amounts of RNA (below detection limit). RNA was directly converted into cDNA with the high-capacity cDNA RT kit (Applied Biosystems, Grand Island, NY) according to manufacturer's recommendations, followed by a 5× dilution with sterile water. RNA yield was qualitatively assessed by checking the Cq value of Beta Actin during QPCR. Analysis was performed on a CFX96 (Bio-Rad Laboratories, The Netherlands) in 2 technical duplicates for each sample with the following protocol: 3-min denaturation at 95 °C, followed by 40 cycles of 15 s at 95 °C and 45 s at 60 °C. After the run, a melting curve was generated from 65 to 95 °C. Total reaction volume was set to 10 μL that consisted of 5 μL iQ™ SYBR® Green Supermix (Bio-Rad, The Netherlands), 250 nM of forward and reverse primers, 2.5 μL of diluted cDNA, and nuclease free water. In prior QPCR experiments, all primers have been tested for efficiency (by serial dilutions) and specificity (by melting curve and gel electrophoresis). After testing various reference

genes (Primer sequences for reference genes and genes of interest are provided in Table S4), Beta Actin and Nono were selected to calculate normalized gene expression using the ΔΔCq method. Differential gene expression was calculated as log2 fold changes compared to vehicle control. Data was clustered and presented as a heatmap with ClustVis (Metsalu and Vilo, 2015). Scaling was disabled and rows clustered using Euclidean distance and Ward linkage, with columns clustered using Euclidean distance and single linkage.

2.8. Data and statistical analysis

In reporter cell line assays, results are expressed as percentages of maximum luciferase or fluorescence activity induced by the reference chemical. In MDC experiments, Nile Red intensities are expressed as fold induction compared to control (DMSO). Data from independent experiments are analyzed in GraphPad (v9.0) by two-way ANOVA with treatment and experiment number as independent variables. No main effect or interaction effect was found for replicate experiments. Subsequently, data is averaged over the independent experiments and used for statistical analysis with one-way ANOVA, employing Dunnett's multiple comparisons test, after the Shapiro-Wilk tests for normal distribution analysis (GraphPad (v9.0)).

Data from MSC experiments is used for benchmark dose (BMD) modeling *via* PROAST Web (v70.1, RIVM, NL) (Hardy et al., 2017). Fold induction values were put in as continuous summary data with standard deviation as dispersion measure. The standard 5% change (corresponding to a 1.05-fold change) was considered not sufficient, therefore critical effect size (CES) was set at 20%, corresponding to a 1.2-fold induction compared to control, as previously used by Norgren et al. (2022). Two different families of models were fit to the data (exponential and Hill), Akaike Information Criterion (AIC) was set to 2, and model averaging was not employed. The resulting confidence intervals were expressed in terms of BMDL and BMDU, the lower and upper bound of the 90% confidence interval, respectively.

3. Results

3.1. Characterization of the 3D model

To study the effects of SSRIs on adipocyte differentiation we chose a 3D MSC adipogenesis model which is reported more physiologically relevant compared to conventional 2D models (Klingelhutz et al., 2018; Shen et al., 2021).

To test this, we characterized the 3D model with a prototypical PPARγ ligand, ROSI as a positive control. We performed H&E staining and confocal imaging, comparing control (DMSO) and ROSI spheroids to examine the morphology of 3D spheroids, including lipid droplet distribution and possible signs of necrosis in the inner core of the spheroid. H&E staining and confocal microscopy confirmed an even distribution of lipid droplets throughout the spheroid without any sign of cell death in the core (Fig. S4a–d). Fluorescence microscopy confirmed increased lipid accumulation with ROSI treatment in 2D (Fig. S4e–f).

ROSI treatment increased the size of 3D spheroids in terms of lipid accumulation but did not affect Hoechst staining, indicating no significant increase in cell proliferation compared to the control (Fig. S4g). When comparing 3D spheroids with 2D monolayer adipocytes, fewer and larger lipid droplets appeared, compared to 2D, indicating a phenotype more similar to *in vivo* adipose tissue, especially visible with ROSI treatments. We tested ROSI from 6 up to 9 concentrations in 2D and 3D and observed a similar induction in both models (Fig. S4h), further confirming the efficiency of the 3D model.

3.2. Application of the 3D model for the assessment of SSRIs

Following characterization, we tested the SSRIs on the 3D model. Where we observed an increase in neutral lipids, an indication of enhanced adipogenesis, with both CIT and SER (Fig. 2a–b). The induction was seen in a concentration-dependent manner, comparable to positive control, the prototypical PPARγ agonist, ROSI.

BMD analysis revealed lower and upper thresholds (BMDL-BMDU) of 1.32–3.27 μM for CIT, and 0.35–0.87 μM for SER, confirming the SSRIs induced adipogenesis in the range of their reported SSCs (0.065–0.65 μM for SER and 0.12–0.92 μM for CIT).

3.3. Effects on endocrine receptors

To test whether enhanced adipogenesis with SSRIs was due to an endocrine mode of action, receptor mediated activity was investigated in agonism and antagonism assays for ER, AR, and DR. SSRIs were tested in at least three biological experiments for both endpoints for each receptor. Each experiment consisted of 3 to 4 plate replicates.

Reference chemicals were included in agonism and antagonism assays for all the receptors. EC50 values calculated for reference agonists (in agonism assays) were used to test antagonistic responses in antagonism assays. Detailed information on experimental set-up and reference chemicals is provided in supplementary data (Table S2), concentration-response curves are shown in Fig. S5a–f. To identify true antagonistic responses that are not due to cytotoxicity cell viability was determined *via* mitochondrial activity (Alamar Blue assay). SER at 30 μM was found to be cytotoxic for both ER-Luc and AR-Luc cells, therefore used at the highest concentration of 10 μM for the following experiments (Fig. S5g). CIT did not decrease cell viability at the highest tested concentration of 30 μM (Fig. S5.)

Estrogenic, androgenic or dioxin-like activity was not observed with CIT or SER at the tested concentrations (data not shown). Additionally, antagonistic activity was not observed on the receptors with either CIT or SER, indicating a different mechanism of action than ER, AR, or DR agonism/antagonism behind their adipogenic effects. Results are summarized in Fig. S5h.

3.4. Results of RNA-seq

To clarify the mechanisms of action of the chemicals, as well as characterizing the 3D model, we performed RNA-seq analysis and compared the transcriptional profiles of cells treated with control (0.1% DMSO), positive control (0.1 μM ROSI) or test chemicals (0.1–1 μM SER, 1–10 μM CIT). Cells treated with control and ROSI were differentiated parallel in 2D and 3D, while SER and CIT treatments were only performed in 3D.

3.4.1. Comparison of the 2D and 3D models

We performed differential expression analysis, comparing first the control and ROSI treatments within the models, in order to assess the differences in the transcriptional profiles of 2D *vs* 3D models. Initial clustering of the data was done with a principal component analysis (PCA) plot based on the different models and treatments, where we found a clear separation between 2D and 3D in PC1 (47.3%) and treatment in PC2 (17.2%). Notably, ROSI treatment showed separate clustering in the same direction compared to the control indicating a similar transcriptional profile (Fig. S6a). Further exploration in DEGs revealed a 50% overlap (2082) between the two models after differentiation with ROSI (Fig. S6b). When looking at the two models within the same treatment the overlap ratio goes up to 61% (4467), highlighting the similar expression profiles of the different models (Fig. S6b).

Subsequently, DEGs were scored based on significance and difference in expression (see above) for gene set enrichment analysis (GSEA) *via* KEGG and GO pathway databases. Most of the pathways were altered similarly after ROSI treatment in both models (Full pathway list is provided as supplementary data). Shortly, metabolic pathways essential for adipogenesis, such as PPAR signaling, were upregulated; while pathways inhibiting adipogenesis, such as Wnt signaling and TGF-beta signaling, were downregulated (Fig. S6.c). Notably, the oxidative

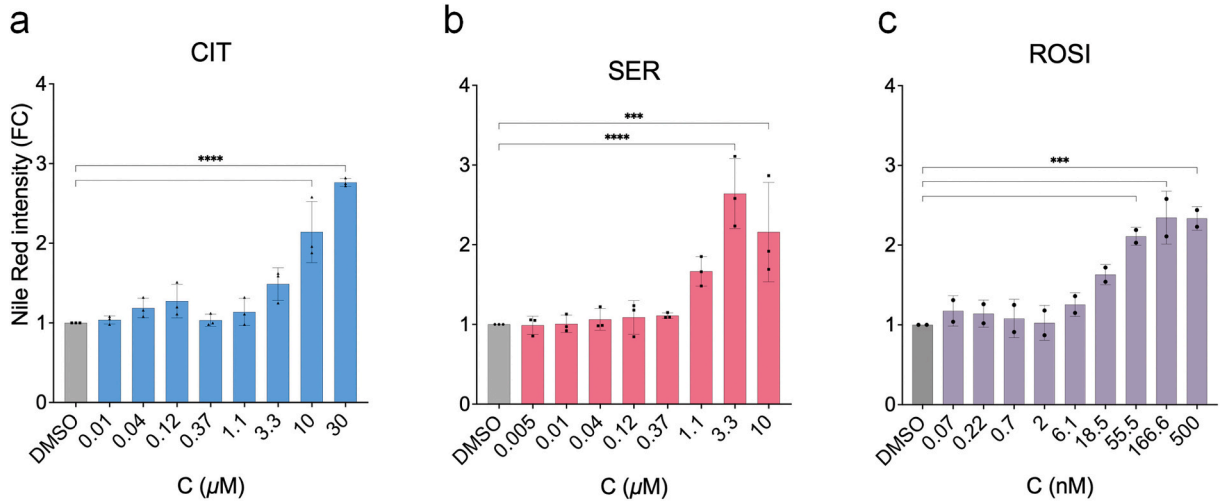

Fig. 2. Increase in neutral lipids during differentiation with (a) citalopram (CIT), (b) sertraline (SER), and (c) rosiglitazone (ROSI), presented as fold change (FC) compared to control (DMSO). Bars represent averages of 3 independent experiments and error bars indicate standard deviation. $^{***}p < 0.005$; $^{****}p < 0.0001$ (GraphPad Prism, v9.0).

phosphorylation pathway was found to be highly upregulated in both models. Although the ribosome pathway was upregulated in 2D and downregulated in 3D with ROSI treatment, it was the strongest upregulated pathway in 3D compared to 2D within the same treatment (data not shown), as shown in a previous study (Shen et al., 2021). According to the functional network of 2D and 3D, adipogenic pathways can be seen clustering together, altered similarly in both models during adipocyte differentiation, confirming the results of the individual pathway analyses (data not shown). Notably, some pathways that could be important in adipogenesis such as adipocytokine signaling and glycerophospholipid metabolism are only significantly upregulated in the functional network of the 3D model, however, this could be the result of using a more stringent threshold for the significant pathways that were used in this particular analysis (FDR < 0.01).

3.4.2. *SSRIs inhibit adipogenic genes and induce lysosomal pathways*

For the SSRIs, differential gene expression analysis revealed a single DEG for SER 0.1 μM, (*IGF-2*: insulin like growth factor 2) which was downregulated, and 134 genes for SER 1 μM, of which 63% (85) were downregulated. CIT treatments mainly resulted in upregulation, 71% (45) of 63 genes were upregulated for CIT 1 μM, and 57% (783) of 1355 genes were upregulated for CIT 10 μM. A total of 23 genes were found overlapping between SER 1 μM and CIT treatments. Among these, there were some associated with adipogenesis or lipid metabolism including adiponectin, lipoprotein lipase, and fatty acid binding protein 4 (*ADIPOQ, LPL, FABP4* respectively). Surprisingly, these were downregulated with all the treatments. Following ranking of genes based on their significance and fold change (see Methods), GSEA analysis revealed a generally reversed gene expression profile compared to the positive control, ROSI (Fig. 3a). Metabolic pathways such as PPAR signaling, non-alcoholic fatty liver disease (NAFLD) and lipid metabolism were found consistently downregulated, in a concentration dependent manner, with the SSRI treatments (Fig. 3a), in the functional network of SER and CIT these pathways can be seen clustering together (Fig. 3b). Notably, the lysosome and related pathways were upregulated by all SSRI treatments (Fig. 3c), and this effect was significant for SER 1 μM and both CIT concentrations (FDR < 0.05). Phagosome and phospholipase D signaling, other pathways related to lysosome function (Corrotte et al., 2006), were significantly affected by CIT at 10 μM (Fig. 3c).

We performed further analyses on the RNA-seq data for an in-depth assessment of the differences in gene expression profiles between ROSI and the SSRIs. Fig. 4a shows the distribution of all genes for each replicate sample, clearly showing the separation between ROSI and SSRI treatments. 3848 genes were significantly affected by at least one of the treatments (FDR < 0.05) and separated into 3 clusters using k-means clustering. Quality of the clustering was confirmed by silhouette scoring, and using the genes within the clusters we performed over representation analysis (ORA), focusing on KEGG pathways. First two clusters both contain metabolic pathways that are upregulated by ROSI and downregulated consistently by SSRI treatments. First cluster consists of 1646 DEGs, leading to 128 enriched pathways. Among these are oxidative phosphorylation and NAFLD pathways, with higher enrichment ratios and lowest FDR values compared to other pathways (Fig. 4b). The second cluster is likely representing adipocyte differentiation with pathways such as PPAR signaling, regulation of lipolysis in adipocytes and other metabolic pathways (Fig. 4b). It consists of 172 mapped genes and 66 enriched pathways in total. The final cluster has the highest number of enriched pathways, with 196 pathways from 750 mapped genes, and contains genes consistently upregulated by SSRIs and downregulated by ROSI, among which the lysosome pathway as one of the most significant pathways (Fig. 4b).

In Fig. 4c violin plots of the representative pathways from each cluster are shown. For the oxidative phosphorylation pathway, the driver genes for the upregulation with ROSI are from complexes III (cytochrome bc_1) and IV (cytochrome *c* oxidase), including *CYC1 (cytochrome c1), COX5A (cytochrome c oxidase subunit 5A), UQCRFS1 (ubiquinol-cytochrome c reductase, Rieske iron-sulfur polypeptide 1), UQCRC2 (ubiquinol-cytochrome c reductase core protein 2)*. Gene expression heatmap in Fig. 4d shows that these genes are downregulated with the SSRIs in a dose dependent manner. The upregulation of PPAR signaling pathway following ROSI treatment is much stronger, as expected. Driver genes for the upregulation with ROSI are involved in adipocyte differentiation, including *PCK1 (phosphoenolpyruvate carboxykinase 1), FABP4 (fatty acid binding protein 4), ADIPOQ (adiponectin), PLIN5 (perilipin 5)* (Fig. 4c). Similarly, with the SSRIs these are downregulated in a dose dependent manner (Fig. 4d). For the lysosome pathway cathepsins *(CTS),* a family of lysosomal proteases, are among the highest upregulated genes with the SSRIs treatments, especially with CIT at 10 μM, while being downregulated by ROSI (Fig. 4c–d).

3.5. *QPCR analysis*

QPCR analysis on selection of adipocyte genes was performed to confirm the findings of RNA-seq. We observed a similar expression profile with QPCR analysis, confirming the results of RNA-seq, with downregulation of genes involved in PPAR signaling after SSRI

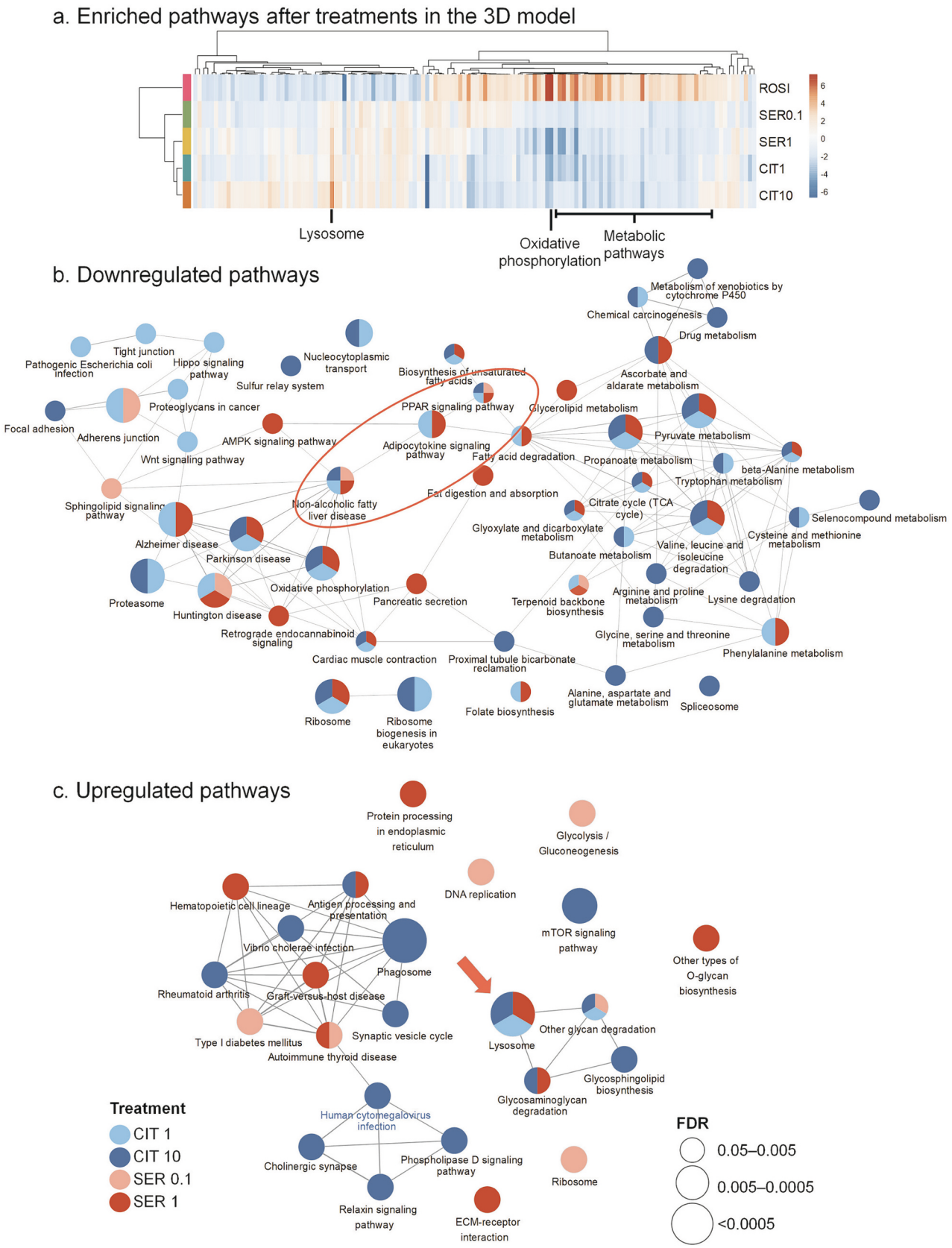

Fig. 3. (a) Annotated heatmap with normalized enrichment scores (NES) of altered Kyoto Encyclopedia of Genes and Genomes (KEGG) pathways after rosiglitazone (ROSI 0.1 μM), citalopram (CIT 1 and 10 μM), and sertraline (SER 0.1 and 1 μM) treatments in 3D. Pathways that are down (blue) or upregulated (red) significantly for at least one of the conditions are shown (FDR < 0.05). Functional network of SER and CIT of (b) down, and (c) upregulated KEGG and gene ontology (GO) pathways (FDR < 0.05). Colors of the circles represent different treatments. Sizes represent significance and are dependent on the smallest FDR value if more than one treatment is significant. (For interpretation of the references to colour in this figure legend, the reader is referred to the web version of this article.)

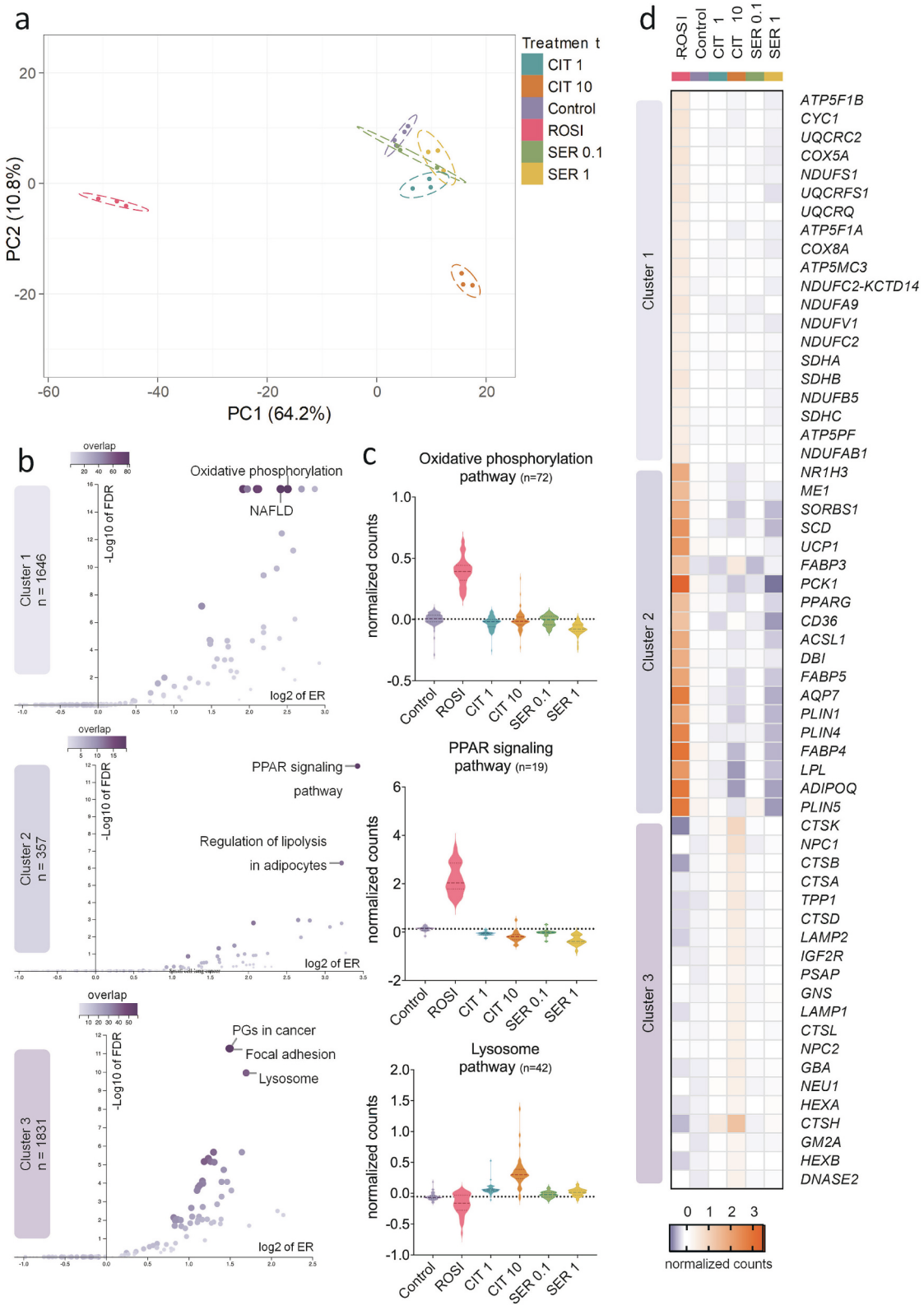

Fig. 4. K-means clustering and pathway analysis: (a) Normalized counts of all genes for each replicate sample (Control (DMSO), rosiglitazone (ROSI), citalopram (CIT 1–10 μM), and sertraline (SER 0.1–1 μM)), presented as principal component analysis (PCA) plot (ClustVis). Ellipses represent the 95% confidence intervals. (b) Annotated pathways with higher enrichment ratio (ER) and significance (n = number of genes per cluster). Scale bar shows the number of overlapping genes between mapped input and gene set. NAFLD: Non-alcoholic fatty liver disease; PPAR: Peroxisome proliferator-activated receptor; PGs: Proteoglycans; FDR: False Discovery Rate. (c) Plots of median-adjusted normalized counts of the genes within representative pathways (*n* = overlap between mapped input and gene set), dashed lines set at median values of control treatment. (d) Heatmap with median-adjusted normalized counts of 20 representative genes from each pathway (GraphPad Prism, v9.0).

treatments, contrary to ROSI (Fig. S7). We also observed upregulation of genes involved in insulin signaling (*INSR* and *IGF1R*) with the SSRIs.

3.6. Effects on 2D MSCs during and after differentiation

In light of the results of the RNA-seq analysis, we performed follow up experiments with functional read-outs in the 2D model, that is more applicable for imaging and plate reader analyses. We first studied the effects of SSRIs on different lipid profiles during and after adipocyte differentiation. We used the 2D MSC adipogenesis model followed by flow cytometry analysis to measure both neutral and phospholipid accumulation by measuring two channels with Nile Red staining (see methods). Fluorescence microscopy image of Nile Red in the two channels shows the separation between lipids (Fig. 5a–d), proving the method's applicability in quantifying both neutral and phospholipids.

As expected, CIT and SER both increased neutral lipids in 2D MSCs during differentiation. However, a much stronger induction was observed in the phospholipid channel with both SSRIs (Fig. 6a–b). BMD modeling confirmed that SSRIs had a stronger effect on phospholipids (Table 2). By comparing BMDs, we observed that SER induced phospholipids at nearly 10 times lower concentrations than neutral lipids.

Furthermore, the effect on phospholipids with SER was observed in a range around reported plasma SSCs (0.065–0.65 μM). Although CIT showed a strong induction in the phospholipid channel, BMD analyses revealed a similar range compared to neutral lipids and above the plasma SSCs (Fig. 6c). Notably, the confidence interval of the BMD of phospholipids was lower compared to neutral lipids, indicating a more accurate estimate of the BMD.

Next, we studied the effects on lysosomes during differentiation *via* LysoTracker Red staining. Here, a strong induction was observed indicating an increase in the formation of lysosomes (Fig. 6d). SSRIs at the tested concentrations led to an induction as high as the positive control, amiodarone.

As the patients receiving SSRI treatment are mostly adults, we performed additional experiments on mature adipocytes. We studied the effects on MSCs after differentiation to see if SSRIs would exert the same effect, changing the lipid profile from neutral lipids to phospholipids. We observed no effect on neutral lipids with the SSRIs after differentiation (Fig. 6e). However, phospholipid levels increased, indicating SSRIs also cause phospholipid accumulation in the lysosomes of mature adipocytes (Fig. 6e).

3.7. Effects on peroxisome proliferator-activated receptors (PPARs)

To test whether the downregulation in the PPAR signaling pathway was due to an effect at the receptor level, we studied the effects of SSRIs on PPARγ and PPARα. Agonist and antagonist activities of SSRIs were tested in at least three independent experiments for both PPARγ and PPARα. Each experiment consisted of 3 to 4 plate replicates.

EC50 values calculated for reference agonists for PPARγ (ROSI) and PPARα (GW7647) (in agonism assays) were used to test antagonistic responses in antagonism assays. T0070907 was used as the reference antagonist for PPARγ. Detailed information on experimental set-up and reference chemicals is provided in supplementary data (Table S2), concentration-response curves are shown in Fig. S8a–c. Cell viability was determined *via* mitochondrial activity (Alamar Blue assay), to identify true antagonistic responses that are not due to cytotoxicity. CIT or SER did not decrease cell viability at the highest tested concentrations (CIT at 30 μM and SER at 10 μM) (data not shown).

Receptor mediated activity was not observed with CIT or SER at the tested concentrations (data not shown), indicating a different mechanism of action than receptor binding behind the SSRIs' downregulatory effect on the PPAR signaling pathway.

4. Discussion

Here, we report the effects of two SSRIs, CIT and SER, on the formation of adipocytes by using a newly set-up human relevant 3D model for adipogenesis from MSC. In combination with whole transcriptomics and functional analyses we were able to pinpoint the mode of action of these chemicals, pointing towards the formation of lysosomes and increased phospholipids, while inhibiting important adipogenic processes, indicating the formation of dysfunctional adipocytes.

To study the effects of the two antidepressants, we first developed a 3D model as there is a growing need for physiologically and human relevant models to assess chemicals' effects on metabolism, including adipogenesis (Legler et al., 2020). Conventional test models often rely on adipogenic progenitor cells, such as the murine preadipocyte cell line 3T3-L1 (Kassotis et al., 2022). As these are already committed to the adipogenic lineage their use only allows for the assessment of adipocyte differentiation. Another limitation of conventional cultures is the common use of 2D monolayers, as there are significant differences in morphology, size, and transcriptional profiles when comparing 2D grown adipocytes to *in vivo* adipose tissue. 3D spheroid models have been developed to improve adipogenic testing and recent studies with murine and human preadipocytes have shown 3D adipogenesis models to be more representative of *in vivo* conditions with improved differentiation and higher adipocyte gene expression (Klingelhutz et al., 2018; Muller et al., 2019; Shen et al., 2021). Although these spheroid models show great improvements over conventional 2D models, these were all developed using adipocyte progenitor cells. On the other hand, mesenchymal stem cells (MSCs) isolated from bone marrow remain multipotent, allowing for the assessment of adipocyte lineage commitment in addition to adipocyte differentiation. In this study, we employed human

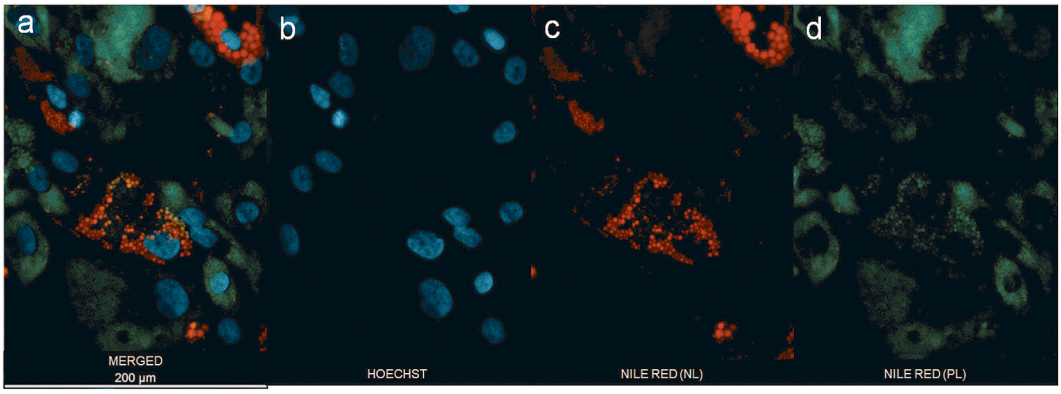

Fig. 5. (a) Fluorescence microscopy image of 2D adipocytes stained with Nile Red and Hoechst for intracellular lipids and cell nuclei, respectively (merged). Scale bar: 200 μm. Split channels showing (b) cell nuclei (DAPI channel), (c) neutral lipids (NL) (FITC channel), and (d) phospholipids (PL) (Texas Red channel). (For interpretation of the references to colour in this figure legend, the reader is referred to the web version of this article.)

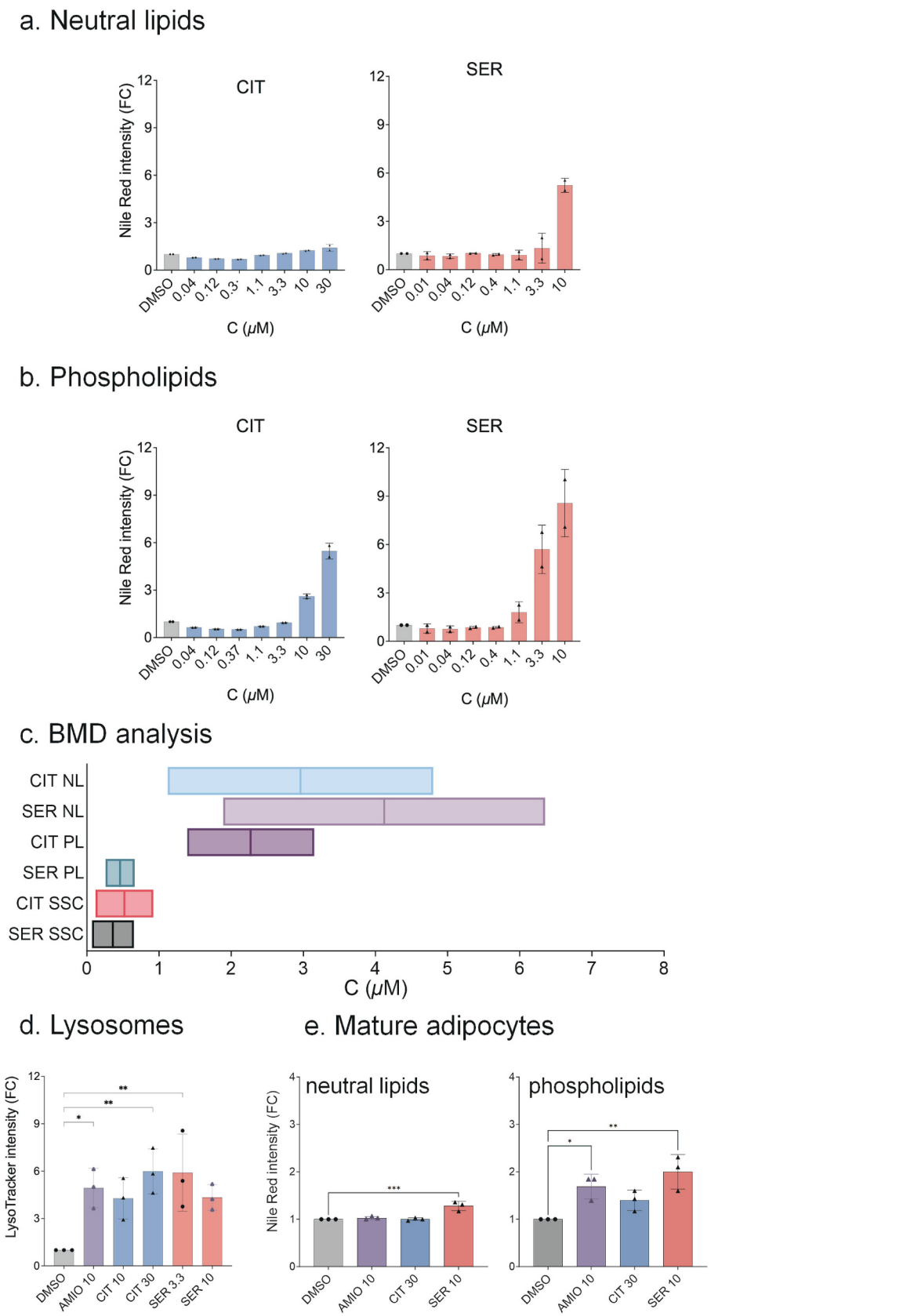

(caption on next page)

Fig. 6. Increase in (a) neutral and (b) phospholipids in 2D MSCs during differentiation with citalopram (CIT), and sertraline (SER). Presented as fold change (FC) compared to control (DMSO). (c) Benchmark dose (BMD) modeling on SSRIs' effects on neutral/phospholipids (NL/PL). Min-max values correspond to 90% confidence intervals (BMDL-BMDU) with ticks at median BMDs. SSC: Steady-state concentrations. (d) Induction of lysosomes in 2D MSCs during differentiation with CIT (10–30 μM), SER (3.3–10 μM), and amiodarone (AMIO 10 μM), presented as fold change compared to control. (e) Increase in neutral and phospholipids in mature adipocytes (2D) by CIT (30 μM), SER (10 μM), and AMIO (10 μM), presented as fold change compared to control. Bars represent averages of 2 to 3 independent experiments and error bars indicate standard deviation. * $p = 0.05–0.005$; ** $p = 0.005–0.0005$; *** $p = 0.0005–0.0001$; **** $p < 0.0001$ (GraphPad Prism, v9.0).

Table 2
Benchmark dose (BMD) for a 20% increase in neutral/phospholipids with SSRIs, including 90% confidence intervals (BMDL-BMDU) and median BMDs (BMD_{MED}).

SSRI	Assay (2D)	BMDL (μM)	BMDU (μM)	BMD_{MED} (μM)
SER	Neutral lipids	1.89	6.35	4.12
	Phospholipids	0.26	0.66	0.46
CIT	Neutral lipids	1.12	4.80	2.96
	Phospholipids	1.39	3.15	2.27

MSCs in a 3D setting with the purpose of improving both human relevance and model applicability, answering the need for a relevant adipogenesis model.

We compared 3D spheroids to 2D grown adipocytes based on phenotype and transcriptional profiles. One of the main concerns in 3D cell models is the formation of a hypoxic core, due to decreased oxygen diffusion towards the center of the spheroid. However, both histological analyses using H&E staining and confocal imaging confirmed an even distribution of lipid droplets throughout the spheroid without any sign of a necrotic core. Moreover, genes involved in hypoxia were not induced, but generally downregulated, such as *SLC2A1*, *VEGFA* and *SERPINE1* (Supplemental data) (Trayhurn et al., 2008). Likely, the limited number of cells allowing rapid diffusion of nutrients and oxygen aided in this observation, compared to previous studies with higher cell numbers (Schmitz et al., 2021). Furthermore, spheroids exposed to ROSI differed from 2D adipocytes in phenotype following differentiation, forming fewer and larger lipid droplets that resemble adipose tissue *in vivo*. This was also shown in multiple publications, as well as transcriptomic profiles that resemble the human situation better than the 2D models (Klingelhutz et al., 2018; Shen et al., 2021). Transcriptional profiles showed quite comparable results after ROSI treatment in both models. However, more pathways related to insulin and adipocytokine signaling, and structural integrity were affected in 3D. Notably, within the same treatment, most pathways were downregulated in 3D compared to 2D. A significant one is TGF-beta signaling pathway, known to inhibit adipogenesis by reducing *PPARγ* expression and CEBPβ activation (Chen et al., 2016). This stronger inhibition in the 3D model might lead to increased adipogenesis, by providing a more suitable setting for the induction of adipogenic genes, as shown in a previous study (Shen et al., 2021). Overall, the novel 3D model shows a more similar phenotype to adipose tissue, and transcriptional profiles indicate a better response to adipogenic stimuli than 2D. Although a direct comparison to human adipose tissue in terms of transcriptional profiles would be the next step to characterize this model, all our analyses indicate it a suitable model for assessing the effects of SSRIs on adipogenesis. In future studies, inclusion of additional cell lines found in adipose tissue, such as macrophages and endothelial cells could enhance the physiological relevance of the model and shed light on the interplay between metabolic organs and immune responses.

Next, we tested the adipogenic properties of CIT and SER and initially observed increased lipid accumulation, an indication of enhanced adipogenesis, with both SSRIs. This effect was observed in a concentration dependent manner, and using a benchmark dose approach points of departure were overlapping with reported plasma SSCs.

To elucidate the underlying mechanism behind SSRIs' effects, we first explored endocrine modes of action. As peroxisome proliferator-activated receptors gamma (PPARγ) is the key regulator of adipogenesis, we studied the agonistic activity on and PPAR gamma and alpha (PPARα). However, agonistic activity was not observed with the CIT and SER on either PPARγ or PPARα. Moreover, we explored the estrogenic, androgenic and dioxin-like activity of SSRIs using receptor cell assays, as there are obesogens shown to increase adiposity *via* such mechanisms. In animal studies prenatal exposure to estrogenic obesogens has been shown to promote the development of obesity in the offspring, occurring through estrogen receptor activation (Darbre, 2017; Heindel et al., 2022; Newbold et al., 2007), additionally, some obesogens with dioxin-like activity have been shown to induce adipogenesis *via* indirectly altering *PPARγ* expression (Casals-Casas and Desvergne, 2011). SSRIs did not exert agonistic or antagonistic effects on ER, AR or DR, suggesting a mechanism beyond direct receptor-mediated activity driving the adipogenic effects.

To further explore the mechanisms, we performed RNA-seq analysis that revealed a distinct gene expression profile in 3D after SSRI treatments compared to the positive control ROSI. To our surprise, key adipogenic genes and important pathways related to adipocyte differentiation (such as PPAR signaling, adipogenesis and fatty acid metabolism) were found downregulated compared to ROSI treatment. In contrast, pathway analyses unveiled upregulation in pathways related to phospholipids and lysosomes with SSRIs, which were confirmed with additional experiments where an induction was observed for both phospholipids and lysosomes. Interestingly, in these additional analyses, the induction in phospholipids was higher compared to neutral lipids in the same model, showing even lower BMD levels as with neutral lipids. We additionally studied the effects of SSRIs on mature adipocytes, as the patients receiving antidepressant treatment are mostly adults, to see if SSRIs would change the lipid profile from neutral lipids to phospholipids. We observed no significant effect on neutral lipids with the SSRIs after differentiation, however, phospholipid levels increased, implying the effects of SSRIs are also apparent in mature adipocytes.

Taking all data together we hypothesized that these SSRIs lead to a common adverse effect of a group of pharmaceuticals, commonly known as cationic amphiphilic drugs (CADs). Shortly, CADs contain a protonable amine group attached to a lipophilic group that allows the unprotonated neutral form to pass through cellular membranes. However, upon reaching an acidic environment the amine group is protonated and no longer able to pass through the membrane, getting "trapped" inside the acidic compartment (Kazmi et al., 2013). Lysosomal trapping *via* this mechanism leads to the inhibition of lysosomal enzymes, specifically lysosomal phospholipase a2 (LPLA2). Located on the lysosomal membrane, LPLA2 is mainly involved in the degradation of lysosomal phospholipids (Hinkovska-Galcheva et al., 2021). Lysosomal accumulation of CADs can result in competitive inhibition of LPLA2, leading to excessive accumulation of lysosomal phospholipids, a process known as drug-induced phospholipidosis (DIP). DIP is mainly shown *in vivo*, with liver and lung being common targets, ultimately leading to pulmonary or liver fibrosis (Hinkovska-Galcheva et al., 2021; Reasor et al., 2006). Considering the existing knowledge on the physiochemical properties of CIT and SER (Reasor et al., 2006), and that both SSRIs were reported to inhibit LPLA2 with a reported IC50 of 8.6 and 19.5 μM, respectively (Hinkovska-Galcheva et al., 2021), our results strongly point towards their lysosomal accumulation in maturing adipocytes, inhibiting LPLA2 to promote phospholipid accumulation. The current gene expression data does not show a difference in LPLA2 expression after SSRI treatment. However, this is not surprising as the inhibition of LPLA2 occurs through a molecular mechanism that is not regulated by

gene expression. Moreover, Kagebeck et al. (2018) tested the effects of a group of CADs (not including CIT or SER, but including amiodarone and another SSRI, fluoxetine) on the differentiation of 3T3-L1 cells. They found that CADs inhibited adipocyte differentiation and that the inhibitory effect showed a strong positive correlation with lysosomal accumulation of the CADs and the inhibition of autophagy within the cells. Autophagy, the process of lysosomal degradation of intracellular components like damaged organelles or proteins, plays a pivotal role in various cellular processes, including lipid metabolism and adipocyte differentiation (Cabrera-Reyes et al., 2021). In this context, they concluded that high accumulation of CADs in lysosomes leads to lysosomal dysfunction and the inhibition of autophagy, which in turn disrupts the process of adipocyte differentiation (Kagebeck et al., 2018). Their findings align with our findings of decreased adipogenesis in MSCs with the SSRIs.

Interestingly, adverse outcome pathways have been developed around lysosomal disruption for liver toxicity (AOP144, lysosome dysfunction; AOP130, phospholipase inhibition) (Kuburic et al., 2023; Oh et al., 2023), in which many key events are present in our data. Apart from lysosome formation, mitochondrial dysfunction is a common key event in both AOPs, similarly, mitochondria function (Oxidative Phosphorylation) was also predicted to be affected in our RNA seq dataset. CADs are also known to accumulate in mitochondria, causing increased proton transfer across the inner mitochondrial membrane towards the matrix, which in turn disrupts electron transfer crucial for ATP synthesis (Fromenty, 2023). Future research with chronic exposure experiments might give insights into further progression of this pathway leading to inflammation and cell death.

The downregulation of many adipocyte related pathways made us hypothesize whether SSRIs were antagonists for PPARγ. However, additional experiments on the PPARγ reporter using an antagonist set-up did not show any effect. Although we do not know exactly how these SSRIs are able to suppress adipogenic pathways, we hypothesize that this could be a compensation for the increased production of phospholipids and a balance towards lysosome formation, leading to less functional adipocytes.

The effects observed in our study are remarkably close to the steady state concentrations observed in clinical studies. These concentrations represent the total concentration of the drug in plasma, which includes both the protein-bound and unbound (free) fractions. Notably, around 80% of CIT is bound to plasma proteins, while the ratio for SER is between 95 and 99% (DeVane, 1999; Pollock, 2001). Moreover, because our system includes proteins from the fetal bovine serum, we cannot precisely know the availability of SSRIs to the MSCs, as we lack knowledge of the chemicals' kinetics in this system. As the unbound fraction in our system might be less than the nominal concentrations added, there is a possibility that BMD values might be an underestimation. Furthermore, a recent publication on physiologically based pharmacokinetic model for CIT estimates that levels in adipose tissue might be more than three times higher than in plasma (Wu et al., 2020). All in all, there is an uncertainty in exposure levels of the bioavailable fraction and further research into the model for *in vitro* to *in vivo* extrapolation, including chemical analysis of such pharmaceuticals in *in vitro* systems, is warranted.

Taken together, our results strongly indicate that CIT and SER are able to disrupt the process of adipogenesis *in vitro* and pave the way for future research directions. To our knowledge there are no reports of effects on adipogenesis *in vivo* following CIT or SER exposures, and future studies should focus on the (developmental) effects of CIT and SER, specifically related to metabolism and associated endpoints such as dyslipidemia, inflammation and fibrosis in adipose tissue using more complex (*in vivo*) models, including mechanistic experiments into the role of LPLA2 in adipocytes.

5. Conclusions

In conclusion, our findings demonstrate the profound impact of CIT and SER on lipid metabolism within differentiating and mature adipocytes in the range of steady-state plasma concentrations. These compounds elicit a cascade of effects, including the disruption of phospholipids and lysosome homeostasis, coupled with the inhibition of adipogenic processes. Contrary to existing epidemiological studies that associate long-term treatment with these compounds with weight gain (Arterburn et al., 2016; Blumenthal et al., 2014; Uguz et al., 2015), our results paradoxically unveil a counterintuitive suppression of adipogenesis on the basis of gene expression. Nevertheless, the systemic consequence of these effects is complex and difficult to predict, yet our data strongly suggest potential implications for the maintenance of a physiologically balanced metabolism. While it is warranted to conduct further investigations to ascertain the translatability of these effects to *in vivo* scenarios, our results underscore the need for heightened caution when employing these pharmaceuticals, particularly during pregnancy.

Funding

This research has received funding from European Union's Horizon 2020 research and innovation program under grant agreement no. 825489, DGK Jubileumfonds of the Faculty of Veterinary Medicine, Utrecht University, and by Tubitak under 2214-A-international doctoral research fellowship program, and Tubitak 1001 research project under grant no. 121S657.

CRediT authorship contribution statement

Deniz Bozdag: Writing – original draft, Visualization, Validation, Software, Investigation, Funding acquisition, Formal analysis, Data curation. **Jeroen van Voorthuizen:** Writing – original draft, Visualization, Software, Investigation, Data curation. **Nikita Korpel:** Writing – original draft, Visualization, Software, Investigation, Data curation. **Sander Lentz:** Visualization, Software, Investigation, Data curation. **Hande Gurer-Orhan:** Writing – review & editing, Supervision, Project administration, Methodology, Funding acquisition, Conceptualization. **Jorke H. Kamstra:** Writing – review & editing, Visualization, Validation, Supervision, Software, Resources, Project administration, Methodology, Funding acquisition, Formal analysis, Data curation, Conceptualization.

Declaration of competing interest

The authors declare that they have no known competing financial interests or personal relationships that could have appeared to influence the work reported in this paper.

Data availability

Sequencing data is available via GEO accession GSE242103

Acknowledgements

Sandra Nijmeijer and Rik van Dellen are gratefully acknowledged for help with cell culture. Richard W. Wubbolts is acknowledged for help with confocal microscopy, Corlinda ten Brink for help with high content imaging. PPARγ and PPARα cell lines (HG5LN-hPPARγ and HG5LN-hPPARα) were kindly provided by Patrick Balaguer, DR2 INSERM, France.

Appendix A. Supplementary data

Supplementary data to this article can be found online at https://doi.org/10.1016/j.taap.2024.116937.

References

Arterburn, D., Sofer, T., Boudreau, D., Bogart, A., Westbrook, E., Theis, M., Simon, G., Haneuse, S., 2016. Long-term weight change after initiating second-generation antidepressants. J. Clin. Med. 5, 48. https://doi.org/10.3390/jcm5040048.

Baumann, P., 1996. Pharmacology and pharmacokinetics of citalopram and other SSRIs. Int. Clin. Psychopharmacol. 11, 5–11. https://doi.org/10.1097/00004850-199603001-00002.

Beyazyüz, M., Albayrak, Y., Eğilmez, O.B., Albayrak, N., Beyazyüz, E., 2013. Relationship between SSRIs and metabolic syndrome abnormalities in patients with generalized anxiety disorder: a prospective study. Psychiatry Investig. 10, 148–154. https://doi.org/10.4306/pi.2013.10.2.148.

Bindea, G., Mlecnik, B., Hackl, H., Charoentong, P., Tosolini, M., Kirilovsky, A., Fridman, W.H., Pagès, F., Trajanoski, Z., Galon, J., 2009. ClueGO: a cytoscape plug-in to decipher functionally grouped gene ontology and pathway annotation networks. Bioinformatics 25, 1091–1093. https://doi.org/10.1093/bioinformatics/btp101.

Blankvoort, B.M.G., De Groene, E.M., Van Meeteren-Kreikamp, A.P., Witkamp, R.F., Rodenburg, R.J.T., Aarts, J.M.M.J.G., 2001. Development of an androgen reporter gene assay (AR-LUX) utilizing a human cell line with an endogenously regulated androgen receptor. Anal. Biochem. 298, 93–102. https://doi.org/10.1006/abio.2001.5352.

Blumberg, B., Egusquiza, R.J., 2020. Environmental obesogens and their impact on susceptibility to obesity: new mechanisms and chemicals. Endocrinology (United States) 161, 1–14. https://doi.org/10.1210/endocr/bqaa024.

Blumenthal, S.R., Castro, V.M., Clements, C.C., Rosenfield, H.R., Murphy, S.N., Fava, M., Weilburg, J.B., Erb, J.L., Churchill, S.E., Kohane, I.S., Smoller, J.W., Perlis, R.H., 2014. An electronic health records study of long-term weight gain following antidepressant use. JAMA Psychiatry 71, 889–896. https://doi.org/10.1001/jamapsychiatry.2014.414.

Cabrera-Reyes, F., Parra-Ruiz, C., Yuseff, M.I., Zanlungo, S., 2021. Alterations in lysosome homeostasis in lipid-related disorders: impact on metabolic tissues and immune cells. Front. Cell Dev. Biol. 9, 1–20. https://doi.org/10.3389/fcell.2021.790568.

Casals-Casas, C., Desvergne, B., 2011. Endocrine disruptors: from endocrine to metabolic disruption. Annu. Rev. Physiol. 73, 135–162. https://doi.org/10.1146/annurev-physiol-012110-142200.

Chamorro-García, R., Sahu, M., Abbey, R.J., Laude, J., Pham, N., Blumberg, B., 2013. Transgenerational inheritance of increased fat depot size, stem cell reprogramming, and hepatic steatosis elicited by prenatal exposure to the obesogen tributyltin in mice. Environ. Health Perspect. 121, 359–366. https://doi.org/10.1289/ehp.1205701.

Chen, Q., Shou, P., Zheng, C., Jiang, M., Cao, G., Yang, Q., Cao, J., Xie, N., Velletri, T., Zhang, X., Xu, C., Zhang, L., Yang, H., Hou, J., Wang, Y., Shi, Y., 2016. Fate decision of mesenchymal stem cells: adipocytes or osteoblasts? Cell Death Differ. 23, 1128–1139. https://doi.org/10.1038/cdd.2015.168.

Corrotte, M., Chasserot-Golaz, S., Huang, P., Du, G., Ktistakis, N.T., Frohman, M.A., Vitale, N., Bader, M.F., Grant, N.J., 2006. Dynamics and function of phospholipase D and phosphatidic acid during phagocytosis. Traffic 7, 365–377. https://doi.org/10.1111/j.1600-0854.2006.00389.x.

Darbre, P.D., 2017. Endocrine disruptors and obesity. Curr. Obes. Rep. 6, 18–27. https://doi.org/10.1007/s13679-017-0240-4.

De Vane, C.L., Liston, H.L., Markowitz, J.S., 2002. Clinical pharmacokinetics of sertraline. Clin. Pharmacokinet. 41, 1247–1266. https://doi.org/10.2165/00003088-200241150-00002.

DeVane, C.L., 1999. Metabolism and pharmacokinetics of selective serotonin reuptake inhibitors. Cell. Mol. Neurobiol. 19, 443–466. https://doi.org/10.1023/A:1006934807375.

Dobin, A., Davis, C.A., Schlesinger, F., Drenkow, J., Zaleski, C., Jha, S., Batut, P., Chaisson, M., Gingeras, T.R., 2013. STAR: ultrafast universal RNA-seq aligner. Bioinformatics 29, 15–21. https://doi.org/10.1093/bioinformatics/bts635.

Edgar, R., Domrachev, M., Lash, A.E., 2002. Gene expression omnibus: NCBI gene expression and hybridization array data repository. Nucleic Acids Res. 30, 207–210. https://doi.org/10.1093/nar/30.1.207.

Fromenty, B., 2023. Discovery of Amiodarone Mitochondrial Toxicity in Liver and beyond, pp. 1–15.

Gafoor, R., Booth, H.P., Gulliford, M.C., 2018. Antidepressant utilisation and incidence of weight gain during 10 years' follow-up: population based cohort study. BMJ (Online) 361, 1–9. https://doi.org/10.1136/bmj.k1951.

Ghaben, A.L., Scherer, P.E., 2019. Adipogenesis and metabolic health. Nat. Rev. Mol. Cell Biol. 20, 242–258. https://doi.org/10.1038/s41580-018-0093-z.

Gill, H., Gill, B., El-Halabi, S., Chen-Li, D., Lipsitz, O., Rosenblat, J.D., Van Rheenen, T.E., Rodrigues, N.B., Mansur, R.B., Majeed, A., Lui, L.M.W., Nasri, F., Lee, Y., Mcintyre, R.S., 2020. Antidepressant medications and weight change: a narrative review. Obesity 28, 2064–2072. https://doi.org/10.1002/oby.22969.

Grün, F., Watanabe, H., Zamanian, Z., Maeda, L., Arima, K., Cubacha, R., Gardiner, D.M., Kanno, J., Iguchi, T., Blumberg, B., 2006. Endocrine-disrupting organotin compounds are potent inducers of adipogenesis in vertebrates. Mol. Endocrinol. 20, 2141–2155. https://doi.org/10.1210/me.2005-0367.

Gutierrez, M., Abramowitz, W., 2000. Steady-state pharmacokinetics of citalopram in young and elderly subjects. Pharmacotherapy 20, 1441–1447. https://doi.org/10.1592/phco.20.19.1441.34851.

Hardy, A., Benford, D., Halldorsson, T., Jeger, M.J., Knutsen, K.H., More, S., Mortensen, A., Naegeli, H., Noteborn, H., Ockleford, C., Ricci, A., Rychen, G., Silano, V., Solecki, R., Turck, D., Aerts, M., Bodin, L., Davis, A., Edler, L., Gundert-Remy, U., Sand, S., Slob, W., Bottex, B., Abrahantes, J.C., Marques, D.C., Kass, G., Schlatter, J.R., 2017. Update: use of the benchmark dose approach in risk assessment. EFSA J. 15, 1–41. https://doi.org/10.2903/j.efsa.2017.4658.

Heindel, J.J., Howard, S., Agay-Shay, K., Arrebola, J.P., Audouze, K., Babin, P.J., Barouki, R., Bansal, A., Blanc, E., Cave, M.C., Chatterjee, S., Chevalier, N., Choudhury, M., Collier, D., Connolly, L., Coumoul, X., Garruti, G., Gilbertson, M., Hoepner, L.A., Holloway, A.C., Howell, G., Kassotis, C.D., Kay, M.K., Ji Kim, M., Lagadic-Gossmann, D., Langouet, S., Legrand, A., Li, Z., Le Mentec, H., Lind, L., Monica Lind, P., Lustig, R.H., Martin-Chouly, C., Munic Kos, V., Podechard, N., Roepke, T.A., Sargis, R.M., Starling, A., Tomlinson, C.R., Touma, C., Vondracek, J., vom Saal, F., Blumberg, B., 2022. Obesity II: establishing causal links between chemical exposures and obesity. Biochem. Pharmacol. 199, 115015 https://doi.org/10.1016/j.bcp.2022.115015.

Hinkovska-Galcheva, V., Treadwell, T., Shillingford, J.M., Lee, A., Abe, A., Tesmer, J.J. G., Shayman, J.A., 2021. Inhibition of lysosomal phospholipase A2 predicts drug-induced phospholipidosis. J. Lipid Res. 62, 100089 https://doi.org/10.1016/J.JLR.2021.100089.

Janesick, A.S., Blumberg, B., 2016. Obesogens: an emerging threat to public health. Am. J. Obstet. Gynecol. 214, 559–565. https://doi.org/10.1016/j.ajog.2016.01.182.

Kagebeck, P., Nikiforova, V., Brunken, L., Easwaranathan, A., Ruegg, J., Cotgreave, I., Munic Kos, V., 2018. Lysosomotropic cationic amphiphilic drugs inhibit adipocyte differentiation in 3T3-L1K cells via accumulation in cells and phospholipid membranes, and inhibition of autophagy. Eur. J. Pharmacol. 829, 44–53. https://doi.org/10.1016/j.ejphar.2018.04.004.

Kamstra, J.H., Hruba, E., Blumberg, B., Janesick, A., Mandrup, S., Hamers, T., Legler, J., 2014. Transcriptional and epigenetic mechanisms underlying enhanced in vitro adipocyte differentiation by the brominated flame retardant bde-47. Environ. Sci. Technol. 48, 4110–4119. https://doi.org/10.1021/es405524b.

Kassotis, C.D., Hoffman, K., Völker, J., Pu, Y., Veiga-Lopez, A., Kim, S.M., Schlezinger, J. J., Bovolin, P., Cottone, E., Saraceni, A., Scandiffio, R., Atlas, E., Leingartner, K., Krager, S., Tischkau, S.A., Ermler, S., Legler, J., Chappell, V.A., Fenton, S.E., Mesmar, F., Bondesson, M., Fernández, M.F., Stapleton, H.M., 2021. Reproducibility of adipogenic responses to metabolism disrupting chemicals in the 3T3-L1 pre-adipocyte model system: an interlaboratory study. Toxicology 461, 1–26. https://doi.org/10.1016/j.tox.2021.152900.

Kassotis, C.D., vom Saal, F.S., Babin, P.J., Lagadic-Gossmann, D., Le Mentec, H., Blumberg, B., Mohajer, N., Legrand, A., Munic Kos, V., Martin-Chouly, C., Podechard, N., Langouët, S., Touma, C., Barouki, R., Ji Kim, M., Audouze, K., Choudhury, M., Shree, N., Bansal, A., Howard, S., Heindel, J.J., 2022. Obesity III: obesogen assays: limitations, strengths, and new directions. Biochem. Pharmacol. 199 https://doi.org/10.1016/j.bcp.2022.115014.

Kazmi, F., Hensley, T., Pope, C., Funk, R.S., Loewen, G.J., Buckley, D.B., Parkinson, A., 2013. Lysosomal sequestration (trapping) of lipophilic amine (cationic amphiphilic) drugs in immortalized human hepatocytes (Fa2N-4 cells). Drug Metab. Dispos. 41, 897–905. https://doi.org/10.1124/dmd.112.050054.

Klingelhutz, A.J., Gourronc, F.A., Chaly, A., Wadkins, D.A., Burand, A.J., Markan, K.R., Idiga, S.O., Wu, M., Potthoff, M.J., Ankrum, J.A., 2018. Scaffold-free generation of uniform adipose spheroids for metabolism research and drug discovery. Sci. Rep. 8, 1–12. https://doi.org/10.1038/s41598-017-19024-z.

Koch, C.M., Chiu, S.F., Akbarpour, M., Bharat, A., Ridge, K.M., Bartom, E.T., Winter, D. R., 2018. A beginner's guide to analysis of RNA sequencing data. Am. J. Respir. Cell Mol. Biol. 59, 145–157. https://doi.org/10.1165/rcmb.2017-0430TR.

Kuburic, M., Gerloff, K., Landesmann, B., 2023. AOP: 144 Endocytic Lysosomal Uptake Leading to Liver Fibrosis [WWW Document]. URL. https://aopwiki.org/aops/144. accessed 12.15.23.

Legler, J., Zalko, D., Jourdan, F., Jacobs, M., Fromenty, B., Balaguer, P., Bourguet, W., Kos, V.M., Nadal, A., Beausoleil, C., Cristobal, S., Remy, S., Ermler, S., Margiotta-Casaluci, L., Griffin, J.L., Blumberg, B., Chesné, C., Hoffmann, S., Andersson, P.L., Kamstra, J.H., 2020. The goliath project: towards an internationally harmonised approach for testing metabolism disrupting compounds. Int. J. Mol. Sci. 21 https://doi.org/10.3390/ijms21103480.

Li, X., Ycaza, J., Blumberg, B., 2011. The environmental obesogen tributyltin chloride acts via peroxisome proliferator activated receptor gamma to induce adipogenesis in murine 3T3-L1 preadipocytes. J. Steroid Biochem. Mol. Biol. 127, 9–15. https://doi.org/10.1016/j.jsbmb.2011.03.012.

Liao, Y., Wang, J., Jaehnig, E.J., Shi, Z., Zhang, B., 2019. WebGestalt 2019: gene set analysis toolkit with revamped UIs and APIs. Nucleic Acids Res. 47, W199–W205. https://doi.org/10.1093/nar/gkz401.

Love, M.I., Huber, W., Anders, S., 2014. Moderated estimation of fold change and dispersion for RNA-seq data with DESeq2. Genome Biol. 15, 1–21. https://doi.org/10.1186/s13059-014-0550-8.

Lustig, R.H., Collier, D., Kassotis, C., Roepke, T.A., Ji Kim, M., Blanc, E., Barouki, R., Bansal, A., Cave, M.C., Chatterjee, S., Choudhury, M., Gilbertson, M., Lagadic-Gossmann, D., Howard, S., Lind, L., Tomlinson, C.R., Vondracek, J., Heindel, J.J., 2022. Obesity I: overview and molecular and biochemical mechanisms. Biochem. Pharmacol. 199, 115012 https://doi.org/10.1016/j.bcp.2022.115012.

Metsalu, T., Vilo, J., 2015. ClustVis: a web tool for visualizing clustering of multivariate data using principal component analysis and heatmap. Nucleic Acids Res. 43, W566–W570. https://doi.org/10.1093/nar/gkv468.

Molenaar, N.M., Bais, B., Lambregtse-van den Berg, M.P., Mulder, C.L., Howell, E.A., Fox, N.S., Rommel, A.S., Bergink, V., Kamperman, A.M., 2020. The international prevalence of antidepressant use before, during, and after pregnancy: a systematic review and meta-analysis of timing, type of prescriptions and geographical variability. J. Affect. Disord. 264, 82–89. https://doi.org/10.1016/j.jad.2019.12.014.

Muller, S., Ader, I., Creff, J., Leménager, H., Achard, P., Casteilla, L., Sensebé, L., Carrière, A., Deschaseaux, F., 2019. Human adipose stromal-vascular fraction self-

organizes to form vascularized adipose tissue in 3D cultures. Sci. Rep. 9, 1–10. https://doi.org/10.1038/s41598-019-43624-6.
Nagy, S.R., Sanborn, J.R., Hammock, B.D., Denison, M.S., 2002. Development of a green fluorescent protein-based cell bioassay for the rapid and inexpensive detection and characterization of Ah receptor agonists. Toxicol. Sci. 65, 200–210. https://doi.org/10.1093/toxsci/65.2.200.
Newbold, R.R., Padilla-banks, E., Snyder, R.J., Phillips, T.M., Jefferson, W.N., 2007. Developmental Exposure to Endocrine Disruptors and the Obesity Epidemic, 23, pp. 290–296. https://doi.org/10.1016/j.reprotox.2006.12.010.
Norgren, K., Tuck, A., Vieira Silva, A., Burkhardt, P., Öberg, M., Munic Kos, V., 2022. High throughput screening of bisphenols and their mixtures under conditions of low-intensity adipogenesis of human mesenchymal stem cells (hMSCs). Food Chem. Toxicol. 161 https://doi.org/10.1016/j.fct.2022.112842.
Oh, J.-H., Yoon, S., Jegal, H., 2023. AOP: 130 Phospholipase A2 (LPLA2) Inhibitors Leading to Hepatotoxicity [WWW Document]. URL. https://aopwiki.org/aops/130. accessed 12.15.23.
Pariente, G., Leibson, T., Carls, A., Adams-Webber, T., Ito, S., Koren, G., 2016. Pregnancy-associated changes in pharmacokinetics: a systematic review. PLoS Med. 13, 1–36. https://doi.org/10.1371/journal.pmed.1002160.
Pollock, B.G., 2001. Citalopram: a comprehensive review. Expert Opin. Pharmacother. 681–698.
Qian, S., Tang, Y., Tang, Q.Q., 2021. Adipose tissue plasticity and the pleiotropic roles of BMP signaling. J. Biol. Chem. 296, 100678 https://doi.org/10.1016/j.jbc.2021.100678.
Reasor, M.J., Hastings, K.L., Ulrich, R.G., 2006. Drug-induced phospholipidosis: issues and future directions. Expert Opin. Drug Saf. 5, 567–583. https://doi.org/10.1517/14740338.5.4.567.
Rogers, J.M., Denison, M.S., 2000. Recombinant cell bioassays for endocrine disruptors: development of a stably transfected human ovarian cell line for the detection of estrogenic and anti-estrogenic chemicals. In Vitro Mol. Toxicol. J. Basic Appl. Res. 13, 67–82.
Ronfeld, R.A., Tremaine, L.M., Wilner, K.D., 1997. Pharmacokinetics of sertraline and its N-demethyl metabolite in elderly and young male and female volunteers. Clin. Pharmacokinet. 32, 22–30. https://doi.org/10.2165/00003088-199700321-00004.
Sarjeant, K., Stephens, J.M., 2012. Adipogenesis. Cold Spring Harb. Perspect. Biol. 4 https://doi.org/10.1101/cshperspect.a008417.
Schmitz, C., Potekhina, E., Belousov, V.V., Lavrentieva, A., 2021. Hypoxia onset in mesenchymal stem cell spheroids: monitoring with hypoxia reporter cells. Front. Bioeng. Biotechnol. 9 https://doi.org/10.3389/fbioe.2021.611837.
Schwartz, M.W., Seeley, R.J., Zeltser, L.M., Drewnowski, A., Ravussin, E., Redman, L.M., Leibel, R.L., 2017. Obesity pathogenesis: an endocrine society scientific statement. Endocr. Rev. 38, 267–296. https://doi.org/10.1210/ER.2017-00111.
Seimandi, M., Lemaire, G., Pillon, A., Perrin, A., Carlavan, I., Voegel, J.J., Vignon, F., Nicolas, J.C., Balaguer, P., 2005. Differential responses of PPARα, PPARδ, and PPARγ reporter cell lines to selective PPAR synthetic ligands. Anal. Biochem. 344, 8–15. https://doi.org/10.1016/j.ab.2005.06.010.
Serretti, A., Mandelli, L., 2010. Antidepressants and body weight: a comprehensive review and meta-analysis. J. Clin. Psychiatry 71, 1259–1272. https://doi.org/10.4088/JCP.09r05346blu.
Shen, J.X., Couchet, M., Dufau, J., de Castro Barbosa, T., Ulbrich, M.H., Helmstädter, M., Kemas, A.M., Zandi Shafagh, R., Marques, M.A., Hansen, J.B., Mejhert, N., Langin, D., Rydén, M., Lauschke, V.M., 2021. 3D adipose tissue culture links the organotypic microenvironment to improved adipogenesis. Adv. Sci. 8, 1–17. https://doi.org/10.1002/advs.202100106.
Shoucri, B.M., Martinez, E.S., Abreo, T.J., Hung, V.T., Moosova, Z., Shioda, T., Blumberg, B., 2017. Retinoid x receptor activation alters the chromatin landscape to commit mesenchymal stem cells to the adipose lineage. Endocrinology 158, 3109–3125. https://doi.org/10.1210/en.2017-00348.
Stirling, D.R., Swain-Bowden, M.J., Lucas, A.M., Carpenter, A.E., Cimini, B.A., Goodman, A., 2021. CellProfiler 4: improvements in speed, utility and usability. BMC Bioinform. 22, 1–11. https://doi.org/10.1186/s12859-021-04344-9.
Trayhurn, P., Wang, B., Wood, I.S., 2008. Hypoxia and the endocrine and signalling role of white adipose tissue. Arch. Physiol. Biochem. 114, 267–276. https://doi.org/10.1080/13813450802306602.
Uguz, F., Sahingoz, M., Gungor, B., Aksoy, F., Askin, R., 2015. Weight gain and associated factors in patients using newer antidepressant drugs. Gen. Hosp. Psychiatry 37, 46–48. https://doi.org/10.1016/j.genhosppsych.2014.10.011.
WHO, 2024. Obesity and Overweight [WWW Document]. URL. https://www.who.int/news-room/fact-sheets/detail/obesity-and-overweight (accessed 3.11.24).
Wu, X., Zhang, H., Miah, M.K., Caritis, S.N., Venkataramanan, R., 2020. Physiologically based pharmacokinetic approach can successfully predict pharmacokinetics of citalopram in different patient populations. J. Clin. Pharmacol. 60, 477–488. https://doi.org/10.1002/jcph.1541.
Xie, C., Jauhari, S., Mora, A., 2021. Popularity and performance of bioinformatics software: the case of gene set analysis. BMC Bioinform. 22, 1–16. https://doi.org/10.1186/s12859-021-04124-5.